

Magnetic hysteresis dynamics of thin Co films on Cu(001)

Jih-Shin Suen, M. H. Lee, G. Teeter, and J. L. Erskine

Department of Physics, The University of Texas at Austin, Austin, Texas 78712

(Received 15 December 1997; revised manuscript received 2 July 1998)

Hysteresis properties of ultrathin (2–4 monolayers) epitaxial Co films grown on Cu(001) surfaces are studied as a function of film thickness, temperature and the strength (H_0), in-plane direction, and frequency (Ω) of applied sinusoidal magnetic field. Scaling of the hysteresis loop area (power loss) of the form $A = A_0 + H_0^\alpha \Omega^\beta \zeta(H, \Omega)$ where ζ is a scaling function is explored. All films exhibit a threshold field (H_t) where switching between equivalent magnetized states is initiated. Hysteresis loop areas measured over five decades in frequency exhibit very weak power-law dependence ($\beta \sim 0.02$). No evidence of a dynamic phase transition is observed and no indication of a low-frequency ($\Omega_0 \sim 10^2$ Hz) characteristic resonance is apparent over the drive frequency range covered. The observed weak power-law scaling does not support results of prior experiments that have been interpreted as corroborating the mean-field Ising model ($\alpha = \beta = \frac{2}{3}$) and continuum spin models of thin-film hysteresis energy-loss scaling. The measured frequency and applied field-dependent scaling of the dynamic coercive force (H_c^*) also appears to be inconsistent with recent phenomenological models of hysteresis behavior based on domain-wall motion that predict that H_c^* scales as $\ln \dot{H}$. The results of this study of Co on Cu(001) and a corresponding study of Fe on W(110) suggest that the dynamics of magnetization reversal in real ultrathin film systems do not exhibit universal behavior in the low-field low-frequency limit. Recent theoretical results based on a more realistic model that accounts for thermal noise and spatial fluctuations in the dynamics yield logarithmic scaling at low Ω and effective exponents β that are compatible with the experiments. A simple physical picture of low drive-frequency energy-loss scaling is described that accounts for the experimental observations. [S0163-1829(99)03505-5]

I. INTRODUCTION

Recent experiments^{1–6} have explored magnetization reversal dynamics in various simple or reduced dimensionality model systems ranging from single-domain nanoparticles¹ to well-characterized epitaxial ultrathin films.^{2–6} Theoretical efforts^{7–21} have studied magnetic hysteresis based on Monte Carlo simulations of lattice Ising models^{7–11} and continuum models,^{12–16} and phenomenological models^{4,5} based on extensions of the classic Néel-Brown^{17,18} model. Recent Monte Carlo simulations¹⁹ based on a kinetic Ising model have successfully simulated domain-wall motion in Fe sesquilayer (1.26 monolayer thick) films on W(110) in which the dynamics are dominated by pinning at second layer island structures. The general objective of these studies has been to test fundamental theories of dynamical scaling, magnetic hysteresis, and magnetic switching, and to gain deeper understanding of the dynamic nonequilibrium processes driven by time-dependent external fields that underlie these phenomena.

While prior measurements performed on individual magnetic particles have been generally inconsistent with thermally assisted magnetization reversal over a single potential barrier (Néel-Brown model), recent work¹ using superconducting quantum interference device microbridge technology applied to single ellipsoidal Co nanoparticles has demonstrated magnetization reversal behavior consistent with a single energy barrier. Switching probability vs time, thermal and field sweeping rate dependences, and activation volume were all found to be compatible with thermal activation over a single energy barrier in a uniformly magnetized uniaxial anisotropy single-domain system. The magnetization rever-

sal process in the Co nanoparticles appears to proceed *via* coherent rotation of spins.

Magnetization reversal in ultrathin films is more complicated than in single-domain nanoparticles. Magnetic sensitive scanning microscopy studies of “unmagnetized” ultrathin films^{22,23} reveal metastable magnetic states consisting of complex domain patterns with domain size ranging from tens to hundreds of microns. An ultrathin magnetic film with uniaxial anisotropy driven by an oscillating external magnetic field, $H(t) = H_0 \sin \omega t$, switches between two stable states that are degenerate in the absence of the applied field ($H_0 = 0$). During the switching process, the system apparently passes through a two-phase (or multiple phase) coexistence regime, characterized by domains where the dynamics can be described by power laws. One important question related to the coexistence regime is: do the dynamical processes associated with magnetization reversal exhibit universal behavior?

Theoretical results obtained from various models and simulations^{7–16,20,21} of ultrathin film magnetization reversal have suggested that the hysteresis loop areas (energy loss per cycle) and other parameters including the dynamic coercive field H_c^* and threshold fields, obey dynamical scaling laws. For example, under certain general assumptions, the hysteresis loop area A has been shown theoretically to obey

$$A \sim H_0^\alpha \Omega^\beta \xi\left(\frac{\Omega}{H_0^\gamma}\right) \quad (1)$$

for all values of H_0 and $\Omega = \omega/2\pi$ where $\xi(x)$ is a scaling function with the properties

$$\xi(x) = \begin{cases} \text{const} & \text{for } x \ll 1 \\ \rightarrow 0 & \text{for } x \gg 1, \end{cases} \quad (2)$$

and α , β , and γ are scaling exponents. The drive field-dependent energy-loss scaling of bulk magnetic materials has been shown to obey the low-frequency limit of Eq. (1). For example, iron and various Permalloy materials obey the Steinmetz law $A \sim B^{1.6}$ for magnetic fields 500–10 000 Oe; at low fields (< 50 Oe), the effective power law for iron is more closely approximated by the Rayleigh law $A \sim B^3$.

Theoretical analysis¹⁰ of a kinetic Ising model based on several different mean-field equations of motion have suggested that in this case the scaling obeys a discontinuous double power law similar to Eq. (1); one valid from the lowest frequencies up to an amplitude-dependent critical value of the frequency $\Omega_c(H)$ and the other valid from this characteristic resonance frequency to the highest frequencies. Direct integration of the (various model-dependent) equations of motion yield hysteresis loops that obey the double scaling laws:

$$A = A_0 + H_0^\alpha \Omega^\beta \xi_l \left(\frac{\Omega}{H_0^\gamma} \right), \quad (3)$$

$$A = H_0^\alpha \Omega^\beta \xi_h \left(\frac{\Omega}{H_0^\gamma} \right), \quad (4)$$

where ξ_l and ξ_h are scaling functions for the low- and high-frequency regimes, and γ is a scaling exponent that depends on the specific kinetics. At low frequencies, $\xi_l(\Omega/H_0^\gamma)$ can be assumed to be a constant [consistent with Eqs. (1) and (2)]; also, Eq. (3) reduces to the form obtained from solving a generic one-dimensional model for a driven bistable system based on a quadratic double-well potential.¹⁶ The Ising model scaling exponents $\alpha = 2/3$, $\beta = 2/3$ and γ are found to be independent of temperature for $T < T_c$, but A_0 was found to be temperature dependent. Recent theoretical work on the scaling of hysteresis in Ising model and cell-dynamical systems has extended prior simulations to consider a linearly rather than a sinusoidally varying external field,²⁰ and disorder.^{20,21} These studies confirm that the scaling falls into two classes, one characterized by Eq. (1) with $\alpha = \beta$ [$O(N)$ symmetry in which the simulations confirm $\alpha = \beta = 1/2$], and the other (mean-field class) characterized by Eq. (3) (in which the simulations confirm $\alpha = \beta = 2/3$). These simulations also suggest that the two-dimensional (2D) Ising model belongs to a different class, and that cell-dynamical systems can manifest a disorder-induced transition similar to the critical point in the 2D Ising model. In the 2D Ising model, for temperature below the critical temperature T_c , or for the coupling constant $J > J_c$ where J_c is a critical value, the simulations yield $A_0 \neq 0$ and $\alpha = \beta = 0.36 \pm 0.08$, with α only weakly dependent on J . For $J < J_c$, $A_0 = 0$ and α increases significantly with J (no single value of α exists).

Several experimental studies of thin-film systems have explored the dynamics of magnetization reversal from the point of view of dynamic scaling based on these specific models. Frequency and applied magnetic-field amplitude-dependent studies of hysteresis loop areas for Fe on Au(001) (Ref. 2) and Co on Cu(001) (Ref. 3) have yielded scaling exponents α and β which are generally compatible with con-

tinuum and Ising-like models, i.e., exponents α , β in the range from 1/2 to 2/3. (Refer to Table I in Ref. 6). These experiments also exhibit characteristic evolution of the shape of hysteresis loops as a function of drive frequency at fixed applied field amplitude. The evolution of loop shape and loop area have been interpreted as being consistent with general features of Eqs. (1)–(4); specifically in the high-frequency limit the scaling functions $\xi(\Omega/H_0^\gamma)$ must eventually approach zero as the response of the magnetic system, characterized by $\langle M(t) \rangle$, can no longer follow the drive field. Based on the evolution of loop shape and area, the experiments on Fe/Au(001) (Ref. 2) and Co/Cu(001) (Ref. 3) suggest that the characteristic frequency Ω_c , that separates the low-frequency scaling regime from the high-frequency regime, lies in the range of 10's of Hz. *This result ($\Omega_c \sim 10^2$ Hz) is clearly inconsistent with experimental results presented in this paper and seems very difficult to reconcile with other work on thin films discussed later.* Luse and Zangwill¹¹ have shown that in a thin-film system dominated by two-dimensional magnetic islands that a characteristic frequency Ω_0 can be associated with the island morphology through the ratio of coverage to mean island perimeter roughness. This model is able to qualitatively account for the experimentally observed frequency dependence of the hysteresis loss for 3 ML Co/Cu(001),³ and the $\pi/2$ phase lag of $\langle M \rangle$ with respect to H at Ω_0 . However, Ω_0 is treated as a parameter in the model, and no attempt is made to evaluate its magnitude from first principles.

Our studies of Fe on W(110) (Ref. 6) and related experimental studies of thicker capped Co films^{4,5} have yielded power-law exponents that depart significantly from the results obtained for uncapped films of Fe on Au(001) (Ref. 2) and Co on Cu(001).³ Furthermore, the latter experiments, as well as the work described in this paper, do not yield any evidence of significant phase lags (of order π) between H and $\langle M \rangle$ that suggest values of $\Omega_c \sim 10$ Hz in the range previously reported.^{2,3} The present paper explores the Co on Cu(001) system in an attempt to resolve the dilemma of what appears to be incompatible experimental results. In addition, our prior results for Fe on W(110) are examined more critically by exploring alternate theoretical frameworks for extracting power-law exponents. We find that while some features of the prior experimental work on the Co/Cu(001) system³ agree with our results, many do not. Specifically, we reproduce hysteresis loop shapes, general values of H_c^* , and the apparent invariance of loop area vs Ω at low frequencies as well as the onset of switching behavior at a critical value of applied magnetic field reported in prior work.³ We also obtain similar loss energy dependence on the drive field strength H_0 at fixed frequency Ω , and observe changes of the coercive force H_c^* as a function of surface roughness. *However, we observe no evidence of power-law scaling exponents at higher frequencies that corroborate Ising-like behavior,³ no evidence of a dynamic phase transition^{2,3} over the frequency range currently accessible in our experiments, and no evidence of low characteristic frequencies in the energy-loss dependence ($\Omega_c \sim 10^2$ Hz).*

We also briefly examine selected phenomenological models of magnetization reversal based on thermally activated domain-wall motion in view of our experimental results for the specific thin-film systems we have studied: $p(1 \times 1)$ Fe

on W(110) and $p(1 \times 1)$ Co on Cu(001). While the phenomenological models appear to provide a meaningful theoretical framework for simulating hysteresis response, there remain significant inconsistencies between the models and general features of existing experimental results including temperature dependences and energy-loss scaling behavior.

II. EXPERIMENT

Our experiments were carried out using an ultrahigh vacuum (UHV) chamber that incorporates Auger electron spectroscopy (AES), low-energy-electron-diffraction (LEED), dual-cell molecular-beam epitaxial growth capabilities and a magneto-optic Kerr effect (MOKE) polarimeter. The samples were mounted at the tip of a liquid-nitrogen dewar that incorporates electron-beam heating permitting sample temperatures ranging from 90 to over 3000 K. Suitable mechanical degrees of freedom permitted sample optical alignment for Kerr effect measurements and positioning for film growth and characterization.

The 1 cm diam. \times 1 mm thick Cu(001) substrate was aligned to $\sim 0.5^\circ$ using x-ray Laue techniques. The (001) surface was mechanically polished (final stage 1 μm diamond paste) including a chemical procedure²⁴ to reduce surface damage. *In situ* cleaning combined repeated sputtering (2 kV Ne at 2×10^{-4} torr, 10 μamp , $\theta_{\text{inc}} = 65^\circ$) followed by annealing (870 K). AES and LEED characterization verified that the preparation procedure produced a clean ($< 1\%$, O, C) well-ordered surface prior to film growth. LEED spot profiles obtained from the Cu(001) surface prior to Co film growth indicated the surface roughness to be compatible with alignment accuracy of 0.5° ; i.e. after sputtering and annealing the center of the crystal yielded spot profile widths limited by the instrument transfer width (~ 100 Å terrace widths) with some deterioration (~ 50 Å terrace widths) near the edge. Monolayer thickness epitaxial Co films were grown by *e*-beam heating a 2 mm diameter 99.95% Co wire. Films were grown on the Cu(001) surface held at 300 K at a rate of 0.1 ML/min in UHV ($P \sim 3 \times 10^{-10}$ torr during growth) and were maintained at $P \sim 5 \times 10^{-11}$ torr base pressure. AES and LEED analysis of the epitaxial film showed low surface impurity concentrations (C, O, S, below 5% combined) and a well-ordered Co layer (range of thickness in the present experiments $2 \text{ ML} \leq \Delta x \leq 4 \text{ ML}$). The thickness of Co films was monitored during film growth by a quartz microbalance located at 1/5 the source-sample distance, and checked using Co and Cu AES peak ratios. Based on past experience in measuring thickness-dependent Curie temperatures, and prior calibration exercises, we judge our quoted thicknesses are accurate to better than $\pm 20\%$. The $p(1 \times 1)$ Fe on W(110) films, that are also discussed,⁶ were prepared and studied using the same instrumentation and similar experimental procedures. The quality of the Fe films on W(110), both smooth and stepped surfaces, is judged somewhat better than most of the Co on Cu(001) films based on the LEED patterns.

In the presentation and discussion of our experimental results, it will become clear that while our experiments were able to reproduce hysteresis loop shapes and certain features of the Co/Cu(001) dynamical response previously measured at low frequencies³ ($\Omega \leq 1$ Hz), significantly different results

were obtained at higher frequencies. We believe that the discrepancies could result from either differences in measurement methodology or from intrinsic differences in the dynamical response of the samples resulting from (for example) differences in thickness, film uniformity, roughness or contamination. This section therefore presents a reasonably detailed description of our MOKE polarimeter including tests and calibrations required to obtain accurate results, and a discussion of issues related to sample differences.

Polarimeter Calibrations: In prior publications,^{25,26} we discussed factors that must be taken into account in order to optimize MOKE polarimeter sensitivity. An optimized polarimeter can achieve detection sensitivity (measured in terms of contrast signal-to-noise ratio) that approaches the statistical limit imposed by the number of detected photons. In order to measure magnetic thin-film dynamical behavior, the MOKE polarimeter frequency response must also be carefully characterized. Our MOKE instrumentation records two cyclic wave forms; one wave form from the photomultiplier tube is proportional to $\langle M(t) \rangle$, the sample magnetization averaged over the region of the magnetic film illuminated by the laser, the second is from a precision noninductive resistor in the magnet circuit which is proportional to the magnet current $i(t)$. At low frequencies, $i(t)$ is in phase and proportional to $H(t)$, the magnetic field in the gap of the in-vacuum magnet. At higher frequencies, magnetic-field amplitude and phase-shift calibrations are required to account for field-amplitude and drive-frequency-dependent changes in the relative phase between $i(t)$ and $H(t)$ resulting from eddy current losses in the magnet and vacuum chamber walls. Phase-shift errors appear directly as errors in the measured dynamic coercive field H_c^* , therefore an accurate calibration procedure is essential to obtain meaningful frequency-dependent hysteresis response results.

The frequency response of our polarimeter (detectors, signal processing electronics, but not including the magnet system) was established using a photoacoustic modulator to impose a variable frequency square wave modulation on the laser beam intensity. The polarimeter response was determined to be independent of frequency with no phase shifts from dc to above 100 kHz. The only calibrations required over the range of frequencies used in experiments reported here involve the magnet response to $i(t)$. The solid core magnet used in prior experiments that studied anisotropy, reorientation transitions, and critical exponents (at low sweep frequencies) was found to be unsatisfactory for MOKE measurements above a few Hz because of large phase shifts between $i(t)$ and $H(t)$, and reduction of the magnetic field in the gap, both effects resulting from eddy currents in the magnet core. To reduce eddy current effects, a UHV-compatible laminated-core electromagnet (stack of 14 mil HyMu80 with mica spacers) was constructed that extended the useful frequency range to over 1 kHz. Our laminated core magnet has 200 turns of kapton-coated copper wire and yields ~ 1000 Oe in a 1.5 cm gap at $i_{\text{dc}} = 20$ amp. The magnet inductance is about 500 μH , and suitable capacitors are used to cancel the inductive reactance at frequencies where $\omega L > R$.

Several methods were used to determine the magnetic-field strength in the gap $H(\Omega, i_m)$ and the relative phase shift $\phi(\Omega, i_m)$ between $i(t)$ and $H(t)$ at a prescribed drive current

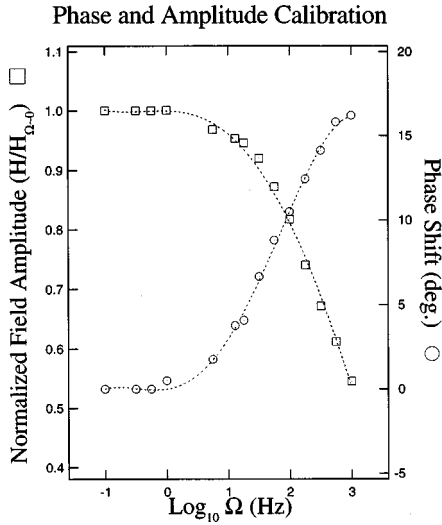


FIG. 1. Plot of relative phase: shift between magnet current and field H , and amplitude $H/H_{\Omega=0}$ vs $\ln \Omega$ for our laminated core magnet at a 10 amp drive current.

amplitude i_m : a Hall probe Gauss meter, a small pick-up loop, and the Faraday effect from a small glass prism placed at the sample location. All methods yielded compatible results. The Hall probe (Bell model 640) probably yielded the most accurate field map in the magnet gap due to the small effective probe area, but the Faraday effect measurement was judged the most accurate means of calibrating the critical phase shift vs driving current frequency and amplitude. Figure 1 displays a typical set of frequency-dependent amplitude and phase-shift calibrations at a fixed sinusoidal drive current for our laminated core magnet. At $\Omega = 1$ kHz and 10 amp magnet current, the field amplitude is reduced to $\sim 0.6 H_{\Omega=0}$, and the relative phase shift between $H(t)$ at the sample and the drive current $i(t)$ is $\phi(\Omega) \sim 16^\circ$. Our solid core electromagnet yielded similar phase shifts around $\Omega = 1$ Hz. Phase-shift calibrations were obtained from a Faraday rotation angle θ_F vs H loop generated using a 3 mm glass prism placed at the location of the thin-film sample. At low frequencies, the polarimeter recorded a linear Faraday rotation vs H response (slope \propto Verdet constant) because the Faraday rotation is proportional to H . At high frequencies, there is no hysteresis from the prism, but phase shifts resulting from vacuum chamber wall and magnet eddy currents produce a slightly elliptical θ_F vs H loop from which the phase shift between $H(t)$ and $i(t)$ can be obtained.

Sample Issues: It is a well established fact that microstructure affects magnetic behavior in both bulk and thin-film materials. The effects can be quite pronounced in ultra-thin films due to the high surface/interface-to-volume ratio. For example, surface steps or roughness can affect anisotropy, and coercive forces, and can produce “rounding” of a phase transition. Surface and thin-film quality become important issues when discrepancies in magnetic behavior are observed in experiments on the same system. Extensive analysis of the relationship between surface roughness and dynamic magnetic behavior for the Co/Cu(001) system^{27–29} provide a very good basis for comparing the quality of films prepared and studied by different groups.

The experiments²⁹ used high-resolution spot profile LEED analysis to characterize three Co/Cu(001) systems

having different degrees of crystal perfection: An ordered smooth film (OS) grown on a Cu substrate having an average terrace width of 300 Å and two other surfaces with greater degrees of substrate roughness produced by light (LSS) or heavy sputtering (HSS). The clean surface terrace widths for the LSS and HSS Cu surfaces were 44 and 10 Å, and the Co film surface terrace widths on all three surfaces were 31 Å (3 ML OS), 25 Å (3 ML LSS), and 12.5 Å (2.5 ML HSS). The coercive forces produced by these three film systems were $H_c = 25$ Oe (3 ML OS), $H_c = 45$ Oe, (3 ML LSS), and $H_c = 1600$ Oe (2.5 ML HSS). Corresponding changes were observed in M_r , the remanent magnetization, and in the threshold field H_t at which hysteresis loops began to open as H_0 was increased. The three Co films produced significantly different values of H_0 -dependent power-law exponents, i.e., 3 ML OS, $\alpha = 0.68$; 3 ML LSS, $\alpha = 1.02$, but not surprisingly large differences.

Our substrates and Co films were prepared to yield the best quality surfaces and films possible using our available capabilities. Stepped Cu surfaces were not studied as in our work on the $p(1 \times 1)$ Fe on W(110) system. Most of our experiments were carried out on 3 ML Co films grown on Cu(001) with an average terrace width of ~ 80 Å, slightly less than the resolving power of our standard LEED system, estimated to be ~ 100 Å. LEED spot profiles of the Co layers on these surfaces indicated a terrace width of 30 Å, similar to that observed by Jiang, Yang, and Wang,²⁹ on their OS Cu(001) substrates even though the substrate roughness was slightly greater for our films. The value of H_c^* at low frequencies for these films was $H_c^* \sim 28$ Oe.

A few measurements were carried out on 3 ML Co/Cu(001) with H_0 applied doing a $[1\bar{1}0]$ direction, the same configuration used by Jiang, Yang, and Wang.³ Additional efforts at alignment and cleaning the Cu(100) crystal resulted in LEED spot profiles that were a little sharper, and essentially limited by the instrument resolving power. Again, the average terrace widths of 3 ML Co/Cu(001) on the slightly smoother Cu substrate was ~ 30 Å, and the dynamic coercive force $H_c^* \sim 23$ Oe was slightly better for films grown on the smoother Cu surface. The threshold field H_t of our films was $H_t \sim 25$ Oe, very similar to the value obtained by Jiang, Yang, and Wang.^{3,29} Based on these observations, we believe that the quality of our films and those of Jiang, Yang, and Wang’s were very similar.

III. RESULTS

We first present and discuss several sets of hysteresis loops. Figure 2 displays three typical sets of magnetic hysteresis loops vs Ω for a 3 ML thick $p(1 \times 1)$ Co film on Cu(001) measured at two different temperatures, two sample orientations and at fixed field amplitude $H_0 > H_c^*$, where H_c^* is defined as the dynamic coercivity. Figure 3 displays corresponding results at a field amplitude $H_0 < H_c^*$. For comparison and future discussion, a similar set of hysteresis loops for 3 ML thick $p(1 \times 1)$ Fe films on W(110) are displayed in Fig. 4. The evolution of loop shape as a function of frequency for loops displayed in Figs. 2–4 fall into three general classes: (1) no perceptible change in shape or area of loop vs Ω , (2) uniform increase in H_c^* vs Ω over the entire

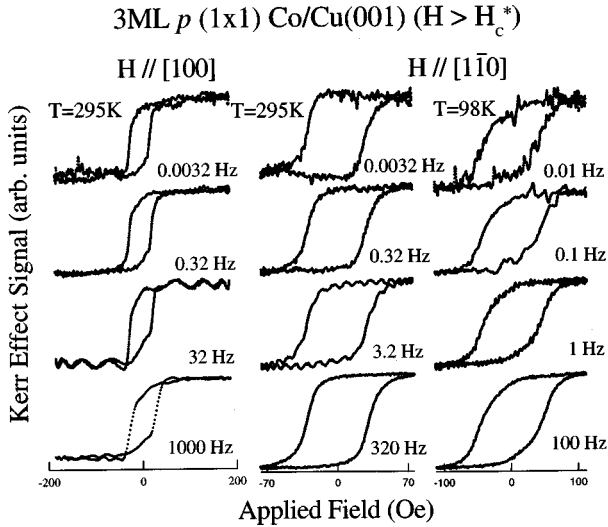


FIG. 2. Representative selection of hysteresis loops for 3 ML thick $p(1 \times 1)$ Co/Cu(001) at two temperatures for $H_0 > H_c^*$ vs drive frequency Ω . Left column, $H_0 = 185$ Oe applied parallel to the $[100]$ in-plane axis; right columns, $H_0 = 80$ Oe ($T = 295$ K), 110 Oe ($T = 95$ K) applied parallel to the $[1\bar{1}0]$ in-plane axis. Discontinuities in the loop trace at low drive frequencies result from fluctuations in light intensity (produced by dust particles or instability in the laser) during the long period required to measure a loop. At higher drive frequencies, integration over many cycles smooths out fluctuations.

range of Ω (where $H_0 > H_c^*$) and (3) uniform increase of H_c^* until $H_c^* = H_0$ at which point the loop abruptly collapses. The Co on Cu(001) loops obey behaviors (1) and (2), the Fe on W(110) loops obey behaviors (2) and (3).

There are important qualitative differences between the hysteresis loop behaviors illustrated in Figs. 2 and 3 for the Co on Cu(001) system and those previously reported for Fe on Au(001) (Refs. 2, 27, 28) and for Co on Cu(001).^{3,29} We note that in Ref. 3, H was applied along the $[100]$ direction. Our experimental results for this configuration are presented

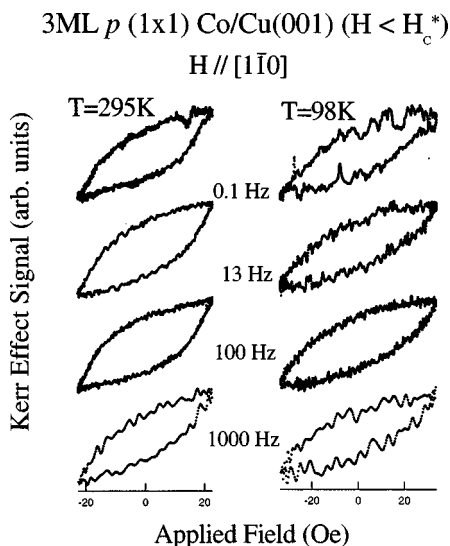


FIG. 3. Hysteresis loops for 3 ML thick $p(1 \times 1)$ Co/Cu(001) at two temperatures for $H_0 < H_c^*$ vs drive frequency Ω . H_0 is applied parallel to the $[1\bar{1}0]$ in plane axis.

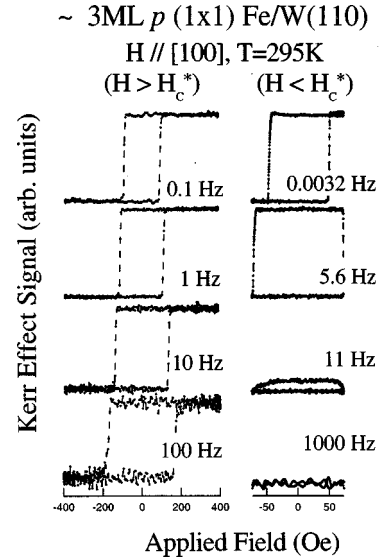


FIG. 4. Hysteresis loops for 3 ML thick $p(1 \times 1)$ Fe/W(001) at $T = 295$ K for $H_0 > H_c^*$ and $H_0 < H_c^*$ vs drive frequency Ω . H_0 is applied parallel to the $[100]$ axis.

in the left column of Fig. 2, but it is clear that there is little or no difference in area scaling for H applied along the $[1\bar{1}0]$ axis which is the easy direction. The in-plane anisotropy is weak. *Our results for Co on Cu(001) exhibit no evidence of the continuous evolution of loop shape observed in prior experiments^{2,3,28,30} and reported in numerical simulations¹² of hysteresis in model spin systems.* In continuum model simulations, evolution of the loop shape is connected with the variation of loop area vs Ω . The area increases, reaching a maximum value at Ω_c , and then decreases monotonically to zero [consistent with the scaling function $\xi(x)$ Eqs. (1), and (2)]. This behavior is indicated (in Fig. 1 of Ref. 3) but is not apparent in our results. Our interpretation of the absence of loop shape evolution is that over the entire frequency range covered by our experiments, the switching dynamics are described by a low-frequency range scaling description [i.e., corresponding to Eq. (1) or Eq. (3) with $\xi(x) = \text{const}$].

A second important difference between our results for Co on Cu(001) and prior experimental work is the power-law behavior of hysteresis loop area vs Ω . The following discussion of frequency-dependent loop areas is qualitative; a more detailed discussion of curve fitting procedures used to extract both H_0 - and Ω -dependent power-law exponents based on specific scaling models is presented in Sec. IV

Figure 5 displays plots of the log of hysteresis loop area A vs $\ln \Omega$ for 2, 3, and 4 ML $p(1 \times 1)$ Co on Cu(001) at two temperatures and for applied field directions along in-plane $[1\bar{1}0]$, and $[100]$ crystal axes. The upper panels correspond to $H > H_c^*$, the lower panels to $H < H_c^*$. Hysteresis loops for 2 and 4 ML thickness (not shown) are essentially the same as for the 3 ML films shown in Figs. 2 and 3. The plots of the log of hysteresis loop area $\log_{10} A$ vs $\log_{10} \Omega$ were used to obtain the power-law exponent β shown as insets on the figures assuming the $x \ll 1$ low Ω limit of Eqs. (1) and (2). The room-temperature data over five decades of Ω appear to yield weak power-law behavior ($\beta \sim .017$) but the low-temperature variation of loop area vs Ω is so weak that it is

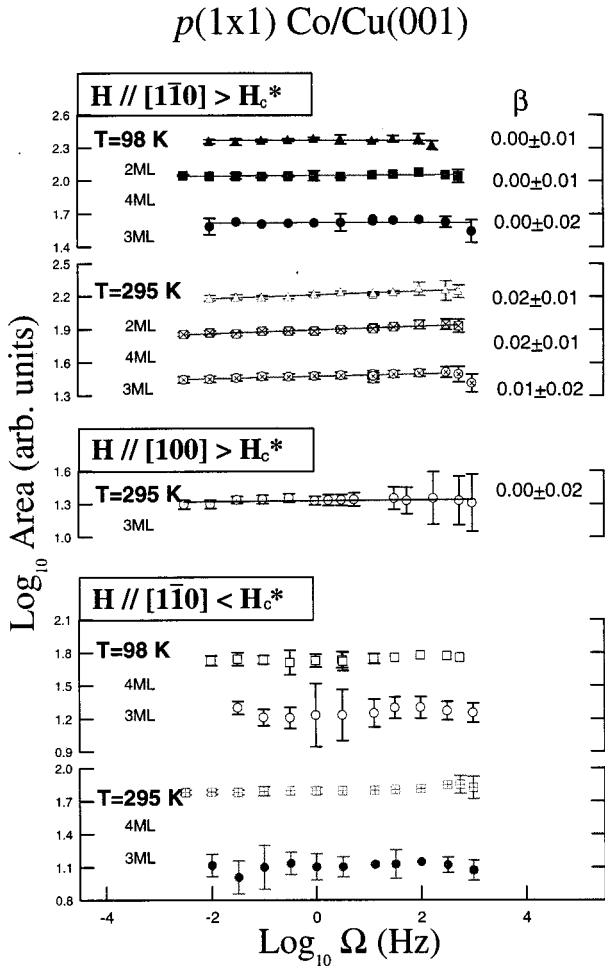


FIG. 5. Plots of log of hysteresis loop area vs $\ln \Omega$ for 2, 3, and 4 ML $p(1 \times 1)$ Co on Cu(001) at two temperatures, and for the two cases $H_0 > H_c^*$ and $H_0 < H_c^*$. The 3 ML hysteresis loops are displayed in Figs. 2 and 3. The exponent β was obtained using dynamic scaling model Eq. (1).

not possible to distinguish between power-law [$1 < 2.4\beta \ln(\Omega_{\max}/\Omega_{\min})$], logarithmic, or other behavior. The fact that we observe a very small value of β can be regarded as being consistent with the “adiabatic” behavior observed below $\Omega \sim 1$ Hz reported previously.³

While our room-temperature results for Co on Cu(001) and both room- and low-temperature results for Fe on W(110) exhibit power-law dependence, our data manifests no evidence of dynamic scaling behavior corresponding to 2D lattice Ising or continuum model predictions: compare exponents in Table I, Ref. 6 in which $\beta \sim 0.3\text{--}0.5$ to the exponents from Co on Cu(001) $\beta \sim 0.017$ or Fe on W(110), $\beta \sim 0.06$. Attempts to reconcile our experimental data with Ising model predictions based on the scaling law Eq. (3) which requires $\alpha = \beta$ also failed.³¹ This point is discussed in greater detail in Sec. IV. *In addition, we observe no abrupt change in power-law behavior in the 3–4 ML thick $p(1 \times 1)$ Co on Cu(001) system corresponding to the previously reported transition³ from adiabatic behavior to power-law scaling with an exponent of $\beta = 0.66$ which was reported to occur around $\Omega = 1$ Hz.*

It is interesting to note that experimental studies of magnetization reversal dynamics in capped ultrathin Co

films^{4,5,32} yield results which are compatible with our results (Figs. 2, 3) for uncapped Co films. In the capped film studies, the accessible frequency range ($0.01 \text{ Hz} \leq \Omega \leq 1 \text{ kHz}$) and driving field strength ($H_0 \leq 1 \text{ kOe}$) produced by an air core solenoid³² were similar to ours. The thin Co films in these studies (8 Å thick) were grown on thick (400 Å) Au layers deposited on natural MoS₂, and capped with a 30 Å Au layer. TEM analysis revealed hexagonal Co crystallites of ~ 100 Å scale, and the magnetic studies showed the films to exhibit strong perpendicular anisotropy. The films were driven into saturation during the magnetization measurements which were all carried out at room temperature. Application of the same power-law scaling function [Eq. (1)] to plots of H_c^* vs $\ln H$ reveal that the power-law exponent β for these films is in the range $\beta \sim 0.02\text{--}0.03$, which is compatible with the results in Fig. 5 obtained using the same scaling law. Application of Eq. (1) scaling to Fig. 5 of Jiang, Yang, and Wang,³ for $H_0 = 92 \text{ Oe}$ yields $\beta \sim 0.26$, over an order of magnitude greater than any of our results on Fig. 5. Application of alternative scaling models to this system are described in Sec. IV. A discontinuous change in the slope of a plot of H_c^* vs $\ln H$ was reported to occur at relatively high frequencies ($\dot{H} = 160 \text{ kOe/s}$) for the 8 ML capped films,³² which was interpreted as an indication of the onset of a change in switching dynamics: The discontinuous power-law behavior was attributed to crossover from wall-motion-dominated reversal to a domain-nucleation-dominated reversal model. We find no evidence of corresponding switching dynamics crossover in our experiments. However, our films are thinner, uncapped, and exhibit in-plane magnetic anisotropy. The upper limit of \dot{H} in our present experiments is approximately $\dot{H} = 300 \text{ kOe/s}$. This limit could lie below the crossover threshold for the uncapped (in-plane anisotropy) 3 ML Co on Cu(001) films studied in our experiments. On the other hand, the similarity of the measured exponents for our (in-plane) films and those measured for thicker capped (perpendicular anisotropy) films suggests that if domain-wall motion dominates magnetization reversal processes in both systems, the wall dynamics as probed by the dynamical exponents β are similar, and not strongly affected by the difference in anisotropy or microstructure.

We carried out several series of hysteresis loop measurements of 2, 3, and 4 ML $p(1 \times 1)$ Co films on Cu(001) vs Ω at 300 and 98 K in which the driving field amplitude H_0 was maintained below H_c^* . The primary motivation for these studies was to explore the possibility that the evolution of loop shape observed in other experiments resulted from driving the films below saturation similar to the loop collapse we observed for $p(1 \times 1)$ Fe on W(110) (Fig. 4). Typical loop shapes are displayed in Fig. 3 and Ω dependences are displayed in the lower plots of Fig. 5. Attempts to obtain meaningful power-law exponents from these loops were unsuccessful. Inspection of the series of loops shows the loop area dependence on Ω is very weak; also, the loop areas tend to be less stable when the thin-film system is driven below saturation. In no case did we observe any “novel” evolution of loop shape vs Ω .

All films [both Fe on W(110) and Co on Cu(001)] exhibited a threshold field effect illustrated in Fig. 6 for 4 ML Co on Cu(001) at 300 K. At a given frequency Ω , and as the

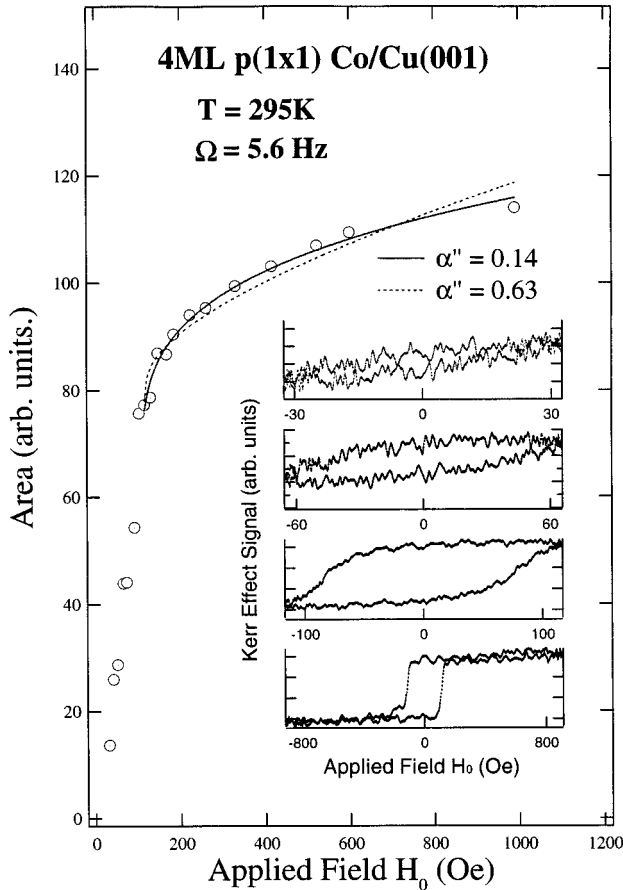


FIG. 6. Plot of the hysteresis loop area A vs applied magnetic field H_0 at fixed Ω and temperature for 4 ML $p(1 \times 1)$ Co on Cu(001). Insets display measured hysteresis loops at selected values of H . Lines through data points show fits for Ising model Eq. (5), the value of the power-law exponent that yields a best fit is $\alpha'' = 0.14$ (refer to Table I).

applied field is increased from very low values to the maximum available field (~ 1 kOe), a threshold field is found where magnetic switching is initiated. Above the threshold, the loop area continues to increase monotonically, and can be fit to a power-law exponent as discussed in the following section. We note that Ω -dependent hysteresis loop scaling for 3 ML $p(1 \times 1)$ Co on Cu(001) was studied for several field amplitudes, and for applied field directions along both high-symmetry directions $[100]$ and $[1\bar{1}0]$ (selected hysteresis loops at four drive frequencies for two cases are displayed in Fig. 2). As later discussed and apparent from Fig. 6, power-law scaling at fixed drive frequency as a function of field amplitude H_0 was found to occur over a range of H_0 extending from below 100 to 1000 Oe. In order to verify that the weak Ω -dependent power-law scaling apparent from the exponents in Fig. 5 are not a result of an inadequate drive field amplitude (below the value where H_0 -dependent scaling is established), experiments were carried out with $H_0 \sim 100$ and 185 Oe.

IV. DISCUSSION

We have presented hysteresis loops and reduced experimental data [i.e., loop area $A(\Omega, H_0)$ vs Ω] for two well-

characterized epitaxial thin magnetic film systems of several thicknesses, for stepped and smooth surfaces,⁶ and two temperatures over a broad range of driving field parameters H_0 and Ω . In the following discussion, we attempt to provide a critical comparison of our experimental results with relevant theoretical models and with other closely related experimental work.

A. Dynamical scaling models and power-law exponents

A primary conclusion of our paper^{6,30} reporting studies of hysteresis dynamics in $p(1 \times 1)$ Fe films on W(110) is that the scaling exponents α and β in the $x \ll 1$ limit of Eq. (1) were significantly different than values obtained from a broad range of theoretical models (Table I in Ref. 6). Adopting an alternate scaling model^{3,21} [$x \ll 1$ limit, Eq. (3)] does not bring the values of exponents obtained from experimental results into agreement with theoretical results³⁰ (discussed below). Prior studies of Co on Cu(001) (Ref. 3) have yielded encouraging agreement with the low-frequency limit of Ising model scaling^{3,16,20} given by Eq. (3):

$$A = \begin{cases} A_0 + K[\Omega^2(H_0^2 - H_{t0}^2)]^{1/3} & H_0 > H_{t0}, \\ 0 & H_0 < H_{t0}, \end{cases} \quad (5)$$

where for fixed H_0 above a switching threshold the area scales as $A = A_0 + K\Omega^{2/3}$. One could argue that application of the pure Ising model to Co/Cu(001) is problematical due to the two orthogonal equivalent easy-axis magnetization directions. It is perhaps more reasonable to assume that the Ising model should apply to the Fe/W(110) system due to the uniaxial anisotropy. Neither of these issues is particularly relevant as we will show that the Ising model, at least in the form embodied by Eqs. (3) or (5), does not appear to provide a valid framework for understanding Ω and H_0 energy-loss scaling in either of the ultrathin film systems under discussion in this paper.

We first review our curve fitting exercises for the Fe/W(110) experimental data. Our original analysis of dynamic scaling for $p(1 \times 1)$ Fe on W(110) was based on the scaling law Eq. (1). We found $\alpha \sim 0.25$ and $\beta \sim 0.03-0.06$. The range of β resulted from examining several film thicknesses at two temperatures ($T = 98$ and 295 K), and both smooth and stepped surfaces. Clearly $\alpha \neq \beta$, suggesting that the power-law scaling at low drive frequencies ($\Omega < 1000$ Hz) is not governed by \dot{H} as required by Eq. (5). The power-law exponent β for $p(1 \times 1)$ Fe on W(110) is very small compared with any of the existing scaling law models (refer to our Table I in Ref. 6).

We also obtained power-law exponents for $p(1 \times 1)$ Fe on W(110) by fitting data to the scaling law Eq. (3), and attempted to fit the data using Eq. (5). This procedure yields values of $\beta \sim 0.1$ similar to those obtained assuming $A_0 = 0$ [i.e., using the scaling of Eq. (1)]. It is clear that the power law obeyed by our data is not consistent with Eq. (5) with $\beta = 2/3$ (Refs. 3 and 11) or $\beta = 0.31$.^{20,21} We carried out fits of the H_0 -dependent scaling data for $p(1 \times 1)$ Fe on W(110) (Fig. 4 of Ref. 6) using Eq. (5) in the form $A = A_0 + K(H_0^2 - H_{t0}^2)^{\alpha/2}$ allowing H_{t0} , A_0 , K , and α to be unrestricted parameters. The results along with corresponding results for the $p(1 \times 1)$ Co on Cu(001) system are presented in Table I.

TABLE I. Summary of typical values for power-law exponents obtained by fitting experimental results to various scaling models. Model (a): power-law exponents α, β obtained by fitting a straight line through data plotted as $\ln A$ vs $\ln \Omega$ and $\ln A$ vs $\ln H$; Model (b): power-law exponent α' was obtained by fitting data allowing A_0 , K , and α' to be free parameters; Model (c): power-law exponent α'' was obtained by fitting data on linear-linear plot of A vs H_0 allowing A_0 , K , H_{t0} , and α'' to be free parameters (refer to Fig. 6). Note that Fig. 6 displays fits corresponding to $\alpha''=0.14$ (lowest χ^2) and $\alpha''=0.63$ (large value of A_0 and χ^2).

Scaling model	System	
	$p(1 \times 1)$ Fe/W(110)	$p(1 \times 1)$ Co/Cu(001)
(a) $A \sim H^\alpha \Omega^\beta$	$\alpha \sim 0.25$	$\alpha \sim 0.15$
(b) $A = A_0 + K \left(\frac{dH}{dt} \right)^{\alpha'}$	$\beta \sim 0.03 - 0.06^a$ $\alpha' \sim 0.12^b$	$\beta \sim 0.01 - 0.02$ $\alpha' \sim 0.05^c$
(c) $A = A_0 + K(H_0^2 - H_{t0}^2)^{\alpha''/2}$	$\alpha'' \sim 0.50$	$\alpha'' \sim 0.14^d$ (see below)

Typical fitting parameters for $\alpha'' \sim 0.14$				
A_0	K	H_{t0}	α''	Deviation χ^2
77.14	0.54	117.0	0.63	81.83
55.66	7.41	113.3	0.31	32.20
33.60	20.26	110.3	0.20	24.72
20.03	29.97	109.2	0.17	22.80
0.01	45.50	107.8	0.14	21.20

^aReference 6.

^bReference 30.

^cThe best fitting parameter is: $A_0 = 75.06$, $K = 35.06$.

It is clear that our experimental results for $p(1 \times 1)$ Fe on W(110) are not consistent with Eq. (5) because $\alpha \neq \beta$, and independent fits of the H_0 and Ω dependent scaling using the more general form Eq. (3) yields $\alpha \sim 0.5$ and $\beta \sim 0.1$. These values are not compatible with any existing analytical results or numerical simulation.

At this point it is useful to comment on the difference in the drive field exponent α obtained from our measurements ($\alpha = 0.14$) and by Jiang, Yang, and Wang^{3,29} $\alpha = 0.67$. It is already clear from the work of Jiang, Yang, and Wang²⁹ that the result $\alpha = 0.67 \sim 2/3$, i.e., the universal value predicted by the mean-field Ising model is a coincidence. The value of α changes appreciably with film roughness $\alpha = 0.67$ for 3 ML OS to $\alpha \sim 1.0$ for 3 ML LSS films, i.e., the value depends on factors other than the system dimensionality. In fact, there is no reason that the same film should not exhibit two or more values of α that describe effective power-law behavior over different drive field ranges. This is certainly true for bulk materials as pointed out in the introduction where for iron, $\alpha = 3$ at low drive fields and $\alpha = 1.6$ for higher drive fields.

The power-law exponents determined by our experiments on $p(1 \times 1)$ Fe on smooth and stepped W(110) exhibit temperature dependence, and depend on the roughness (step density) of the substrate. We found it impossible to account for the measured temperature dependence based on a scaling model consistent with the mean-field Ising results Eq. (3) allowing A_0 to be temperature dependent, $A = A_0(T) + K\Omega^\beta$ even when β was allowed to depart significantly from the Ising model values.

Analysis of our experimental results lead to the conclu-

sion that the continuum and lattice Ising models being used to study hysteresis dynamics in generic magnetic systems fail to address the intrinsic factors that govern the energy-loss scaling in the $p(1 \times 1)$ Fe on W(110) system. The same conclusion must also apply to the $p(1 \times 1)$ Co on Cu(001) system: Our experimental results for Co on Cu(001) require $\beta \ll \alpha$, therefore we attach no special meaning to the power-law exponents in terms of, for example, the Ising model.

The abrupt collapse of hysteresis loops for $p(1 \times 1)$ Fe on W(110) at fixed H_0 and at a critical value of Ω defined by $H_c^*(\Omega) > H_0$ is a feature of thin-film dynamical behavior of the Fe/W(110) system that is different from the behavior of the Co/Cu(001) system. This collapse may simply be a manifestation of the strong uniaxial anisotropy of the $p(1 \times 1)$ Fe on W(110).

B. Phenomenological models based on wall dynamics

Hysteresis dynamics of the previously mentioned Au capped perpendicular anisotropy Co films were simulated using a phenomenological model.^{4,5} The model is based on thermally activated relaxation (single relaxation time approximation) and assumes that the activation energy for magnetization reversal varies linearly with the applied magnetic field. Assuming a driving field described by dH/dt , the equations describing dM/dt can be integrated to yield $M(H)$, from which an expression of the dynamic coercive field H_c^* is obtained from solving $M(H_c^*) = 0$:

$$H_c^*(\Omega, H, T) = \frac{kT}{V^* M_s} \ln \dot{H} + C. \quad (6)$$

In Eq. (6), C is a constant independent of the sweep rate \dot{H} , V^* is a characteristic switching (Barkhausen) volume, M_s is the saturation magnetization and kT is the Boltzmann constant multiplied by temperature.

The model has been used to draw reasonable conclusions from simulating experimentally determined hysteresis loops and measurements of $H_c^*(\Omega)$ for Co films^{4,5} and Co rare-earth films.³³ We judge that the precision of our experimental data (hysteresis loops) should be improved before seriously attempting to explore domain-wall nucleation and motion based on this model^{4,5} and extensions³³ of it. Here we wish only to point out that typical values for α and β that we have obtained for 2 ML $p(1 \times 1)$ Fe on W(110) (Ref. 6) $\beta \sim 0.093$, $\alpha \sim 0.25$ are incompatible with the scaling predicted by Eq. (6) which requires $\alpha = \beta$.

C. Relation to dynamical models for thin films (thickness $\sim 1000 \text{ \AA}$)

An extensive scientific literature covering dynamically driven domain-wall motion in an intermediate film thickness range (several hundreds to thousands of angstroms) has resulted from research related to magnetic recording heads and sensors. Numerical simulations^{34,35} of domain-wall dynamics based on solutions of the Landau-Lifshitz equation with phenomenological damping yield complex wall motion behavior including periodic transitions between Bloch and Néel walls and the formation of multiple vortices. The simulations also yield predictions of power-law scaling exponents at low frequencies describing frequency-dependent hysteresis loss as well as manifestations of phase lags at high frequencies:³⁵ departure of hysteresis loss scaling from the low-frequency limit power-law dependence [Eq. (1) with $\xi(x) = \text{const}$] accompanied by striking evolution of the dynamic hysteresis loops similar to those predicted based on cell dynamical simulations in 2D Ising systems.¹⁴ In the numerical simulations of 2000 \AA thick Permalloy films ($H_{c \text{ max}}^* \sim 2.5 \text{ Oe}$), the hysteresis loss is found to scale as $A \propto \Omega^\beta$ with $\beta = 1.1$ [primarily resulting from the increase of $H_c^*(\Omega)$] up to $\dot{H} \sim 1.5 \times 10^9 \text{ Oe/s}$ where the loop begins to become elliptical and then collapses at higher values of \dot{H} . The frequency scale that sets the $\zeta \rightarrow 0$ limit of power-law scaling and the onset of significant phase lags between M and H is the point at which the gyromagnetic spin precession no longer follows the external drive field. If the same fundamental limit applies to ultrathin films, it is not surprising that our experimental results for $p(1 \times 1)$ Fe on W(110), or $p(1 \times 1)$ Cu on Cu(001) do not exhibit evidence of crossover from the low-frequency limit $\xi(x) = \text{const}$ to a regime where the scaling function begins to dominate the power-law behavior. Our accessible range of \dot{H} extends to $\dot{H}_{\text{max}} \sim 3 \times 10^6 \text{ Oe/s}$; clearly the low-frequency range by the above criteria.

V. CONCLUSIONS

Our experimental results differ in substantive features with prior experimental work that reportedly corroborates existing theoretical models of the dynamic scaling of hysteresis behavior in ultrathin films. Our experiments detect no evidence of the evolution of hysteresis loop shapes corre-

sponding to the onset of significant phase lags between $\langle M(t) \rangle$ and $H(t)$ in the frequency range covered ($\Omega_{\text{max}} \sim 1 \text{ kHz}$, $\dot{H}_{\text{max}} \sim 3 \times 10^6 \text{ Oe/s}$). Weak power-law behavior (small β) was measured in all cases with no evidence of a significant (discontinuous) change in power-law behavior suggesting a signature of the 2D Ising model ($\beta \sim 2/3$) or crossover between distinct dynamical regimes (no evidence of a dynamic phase transition other than the collapse of loops when $H < H_c^*$). The loop scaling for the Fe films on W(110) depends both on surface or interface roughness and temperature. This suggests that the power-law scaling is not universal. The surface step (roughness) dependence of energy-loss scaling suggests that domain nucleation and/or wall motion are affected by steps—possibly providing nucleation or pinning centers. The temperature dependence of the $p(1 \times 1)$ Fe on the W(110) system is compatible with predictions based on the 2D Ising model [Eq. (3) in the $\xi(x) = \text{const}$ limit] in the sense that a temperature-dependent A_0 term obtained from fitting experimental data changes with the correct sign. However, the power-law exponent is incorrect by at least a factor of 3.

The general consistencies¹⁹ between power-law exponents (Table I, Ref. 6) obtained from similar or identical theoretical models using several approaches (numerical simulations and analytical solutions for example) suggest that the models are valid within the limits of assumptions they are based on. The failure of these models to properly account for measured frequency-dependent energy-loss scaling in ultrathin films reflects the complexity of the underlying dynamical processes. Valid models will probably require dealing with the dependence of domain nucleation and wall motion on intrinsic and extrinsic defects and temperature. Judging from the weak frequency-dependent scaling accompanied by finite and strongly temperature-dependent hysteresis loss measured by our experiments, our measurements could be a manifestation of dynamics dominated by a common low-frequency regime mechanism.

Recent theoretical work has yielded very encouraging agreement with our measurements of dynamic scaling.^{36–38} Magnetic hysteresis for a two-dimensional spin- $\frac{1}{2}$ nearest-neighbor kinetic Ising model was investigated using Monte Carlo simulations and analytical theory. The model takes into account thermal noise and spatial fluctuations in the order parameter by considering the magnetization to reverse through random nucleation of single droplets of spins aligned with the applied field. The model predicts magnetic response that is qualitatively different from what is obtained from mean field models or in simulations of spatially extended systems. One of the principal results of these calculations is that the average hysteresis loop area exhibits an extremely slow crossover to logarithmic dependence at low drive frequencies. The crossover is slow enough that the frequency dependence can easily be mistaken for power-law dependence even when several decades of response are measured. *More importantly, the effective power-law exponents obtained from both the analytical calculations and Monte Carlo simulations in the range covered by our experiments (second to μs time scales) are $\beta \sim 0.077$, basically in the range measured by our experiments.* The characteristic frequencies (Ω_c) in these theoretical models also appear to be quite high.

It is not difficult to account for strong field strength-dependent hysteresis loss accompanied by weak frequency-dependent scaling in a magnetic system (i.e., $\beta \ll \alpha$). It is reasonably well established (although not in ultrathin films) that domain-wall velocities saturate (maximum velocities $v_0 \sim 10\text{--}20 \times 10^3$ cm/s in low coercivity 500 \AA thick permalloy films for H above a few 10^3 Oe). Any power loss that scales with domain-wall velocities would yield weak scaling with Ω if wall velocity saturation governs the loss in a particular dynamical regime. At low drive frequencies one can imagine the energy loss being produced by individual Barkhausen jumps in which a domain configuration changes abruptly in response to thermal activation at the applied field strength. If dH/dt is slow, the energy produced by the domain jump is $\Delta E \sim H \Delta M$, where $\Delta M/dt$ is related to a domain-wall jump. In this low-frequency regime, the energy loss will appear to be independent of Ω , but will clearly be dependent on H_0 because each pinning site will have a temperature and applied field-dependent probability for a Barkhausen jump.

A more sophisticated way of describing this physical model is to consider phenomenological models based on a relaxation time in which nucleation and domain-wall processes are characterized by

$$\tau = \tau_0 \exp \left[\frac{V^* M_s}{kT} (H - H_c)^\gamma \right],$$

where τ is the relaxation time, $1 < \gamma < 2$ is a model-dependent parameter, and the other symbols are defined as for Eq. (6). In these models, the dynamics are slow if $V^* M/kT$ is large (weak dynamic scaling). However, the temperature dependence of H_c can be large, being dependent on the thermal dependence of the anisotropy; thus weak dynamic scaling is not necessarily inconsistent with a strong temperature dependence of H_c^* .

We believe the key to improving our understanding of hysteresis dynamics lies in expanding the parameter space covered by the measurements (higher H , broader Ω range, and wider temperature range, including measurements near T_c) and careful experiments on model systems in which direct measurements of characteristic domain sizes, domain nucleation dynamics and wall velocities can be carried out. These experiments are becoming feasible, and should help guide development of more realistic theoretical models of switching dynamics and hysteresis in ultrathin film magnetic systems.

ACKNOWLEDGMENTS

This work was supported by NSF DMR-9623494 and The Robert A. Welch Foundation.

-
- ¹W. Wernsdorfer, E. Bonet Orozco, K. Hasselbach, A. Benoit, B. Barbara, N. Demoncey, A. Loiseau, H. Pascard, and D. Mailly, *Phys. Rev. Lett.* **78**, 1791 (1997).
- ²Y.-L. He and G.-C. Wang, *Phys. Rev. Lett.* **70**, 2336 (1993).
- ³Q. Jiang, H.-N. Yang, and G.-C. Wang, *Phys. Rev. B* **52**, 14 911 (1995).
- ⁴B. Raquet, R. Mamy, and J. C. Ousset, *Phys. Rev. B* **54**, 4128 (1996).
- ⁵P. Bruno, G. Bayreuther, P. Beauvillain, C. Chappert, G. Lugert, D. Renard, J. P. Renard, and J. Seiden, *J. Appl. Phys.* **68**, 5759 (1990).
- ⁶Jih-Shin Suen and J. L. Erskine, *Phys. Rev. Lett.* **78**, 3567 (1997).
- ⁷D. Dhar and P. B. Thomas, *J. Phys. A* **25**, 4967 (1992); *Europhys. Lett.* **21**, 965 (1993).
- ⁸M. Acharyya and B. K. Chakrabarti, *Phys. Rev. B* **52**, 6550 (1995).
- ⁹W. S. Lo and R. A. Pelcovits, *Phys. Rev. A* **42**, 7471 (1990).
- ¹⁰C. N. Luse and A. Zangwill, *Phys. Rev. E* **50**, 224 (1994).
- ¹¹C. N. Luse and A. Zangwill, *J. Appl. Phys.* **79**, 4942 (1996).
- ¹²M. Rao, H. R. Krishnamurthy, and R. Pandit, *Phys. Rev. B* **42**, 856 (1990); M. Rao and R. Pandit, *ibid.* **43**, 3373 (1991).
- ¹³A. M. Somoza and R. C. Desai, *Phys. Rev. Lett.* **70**, 3279 (1993).
- ¹⁴S. Sengupta, Y. Marathe, and S. Puri, *Phys. Rev. B* **45**, 7828 (1992).
- ¹⁵F. Zhong, J. X. Zhang, and G. G. Siu, *J. Phys.: Condens. Matter* **6**, 7785 (1994); F. Zhong and J. X. Zhang, *Phys. Rev. Lett.* **75**, 2027 (1995).
- ¹⁶P. Jung, G. Gray, R. Roy, and P. Mandel, *Phys. Rev. Lett.* **65**, 1873 (1990).
- ¹⁷L. Néel, *Ann. Geophys. (C.N.R.S.)* **5**, 99 (1949).
- ¹⁸W. F. Brown, *Phys. Rev.* **130**, 1677 (1963).
- ¹⁹M. Kolesik, M. A. Novotny, and P. A. Rikvold, *Phys. Rev. B* **56**, 11 791 (1997).
- ²⁰Z. Fan, Z. Jinxiu, and L. Xiao, *Phys. Rev. E* **52**, 1399 (1995).
- ²¹F. Zhong, J. Dong, and D. Y. Xing, *Phys. Rev. Lett.* **80**, 1118 (1998).
- ²²H. P. Oepen, *J. Magn. Magn. Mater.* **93**, 116 (1991).
- ²³H. P. Oepen and J. Kirschner, *Scanning Microsc.* **5**, 1 (1993).
- ²⁴J. S. Ahearn, Jr., J. P. Monaghan, and J. W. Mitchell, *Rev. Sci. Instrum.* **41**, 1853 (1970).
- ²⁵R. L. Fink, C. A. Ballentine, J. L. Erskine, and José Araya-Pochet, *Phys. Rev. B* **41**, 10 175 (1990).
- ²⁶S. D. Bader and J. L. Erskine, in *Ultrathin Magnetic Structures II*, edited by B. Heinrich and J. A. C. Bland (Springer-Verlag, Berlin, 1994), Chap. 4.
- ²⁷Y. L. He and G.-C. Wang, *J. Appl. Phys.* **76**, 6446 (1994).
- ²⁸Y.-L. He, Y.-F. Liew, and G.-C. Wang, *J. Appl. Phys.* **75**, 5580 (1994).
- ²⁹Q. Jiang, H.-N. Yang, and G.-C. Wang, *J. Vac. Sci. Technol. B* **14**, 3180 (1996).
- ³⁰Q. Jiang, H. N. Yang, and G. C. Wang, *J. Appl. Phys.* **79**, 5122 (1996).
- ³¹J. L. Erskine and Jih-Shin Suen, *Phys. Rev. Lett.* **80**, 1119 (1998).
- ³²B. Raquet, M. D. Ortega, M. Goiran, A. R. Fert, J. P. Redoules, R. Mamy, J. C. Ousset, A. Sdaq, and A. Khmou, *J. Magn. Magn. Mater.* **150**, L5 (1995).
- ³³S. S. Malhorta, Z. S. Shan, D. C. Stafford, S. H. Liou, and D. J. Sellmyer, *IEEE Trans. Magn.* **32**, 4019 (1996).

³⁴S. W. Yuan and H. N. Bertram, Phys. Rev. B **44**, 12 395 (1991).

³⁵S. W. Yuan and H. N. Bertram, J. Appl. Phys. **72**, 1033 (1992).

³⁶S. W. Sides, P. A. Rikvold, and M. A. Novotny, Phys. Rev. E **57**, 6512 (1998).

³⁷S. W. Sides, P. A. Rikvold, and M. A. Novotny, Phys. Rev. Lett. **81**, 834 (1998).

³⁸S. W. Sides, P. A. Rikvold, and M. A. Novotny, J. Appl. Phys. **83**, 6494 (1998).